Naval Research Laboratory
Washington, DC 20375-5000

NRL Memorandum Report 6811

Use Of A Zone Model For Validation Of A Horizontal Ceiling/Floor Vent Algorithm

J. L. BAILEY, F. W. WILLIAMS AND P. A. TATEM

Navy Technology Center for Technology and Survivability
Chemistry Division

April 26, 1991

REPORT DOCUMENTATION PAGE

Form Approved
OMB No 0704-0188

1. AGENCY USE ONLY (Leave blank)	2. REPORT DATE	3. REPORT TYPE AND DATES COVERED
	1991 April 26	Memorandum Report

4. TITLE AND SUBTITLE
Use of a Zone Model for Validation of a Horizontal Ceiling/Floor Vent Algorithm

5. FUNDING NUMBERS
62121N
RH21522

6. AUTHOR(S)
J. L. Bailey, F. W. Williams and P. A. Tatem

7. PERFORMING ORGANIZATION NAME(S) AND ADDRESS(ES)
Naval Research Laboratory
Washington, DC 20375-5000

8. PERFORMING ORGANIZATION REPORT NUMBER
NRL Memorandum Report 6811

9. SPONSORING/MONITORING AGENCY NAME(S) AND ADDRESS(ES)
Office of Naval Technology
Arlington, VA 22217

10. SPONSORING/MONITORING AGENCY REPORT NUMBER

11. SUPPLEMENTARY NOTES

12a. DISTRIBUTION/AVAILABILITY STATEMENT
Approved for public release; distribution unlimited.

12b. DISTRIBUTION CODE

13. ABSTRACT *(Maximum 200 words)*

A zone model is used to test the validity of a horizontal ceiling/floor vent flow algorithm. Development of this algorithm makes it possible to fully characterize vertical flow through a horizontal vent. The algorithm is incorporated into a computer model written to simulate a compartment, with a fire inside, ventilated only through a hole in the ceiling. Model predictions are shown to be comparable to small scale experimental results. To further test and confirm this algorithm, a similar comparison should be made on a larger scale.

14. SUBJECT TERMS
Modeling algorithms; Fire modeling; Computer models
Zone modeling; Vent flow; Enclosed spaces

15. NUMBER OF PAGES
43

16. PRICE CODE

17. SECURITY CLASSIFICATION OF REPORT	18. SECURITY CLASSIFICATION OF THIS PAGE	19. SECURITY CLASSIFICATION OF ABSTRACT	20. LIMITATION OF ABSTRACT
UNCLASSIFIED	UNCLASSIFIED	UNCLASSIFIED	SAR

NSN 7540-01-280-5500

Standard Form 298 (Rev 2-89)
Prescribed by ANSI Std 239-18
298-102

CONTENTS

USE OF A ZONE MODEL FOR VALIDATION OF A HORIZONTAL CEILING/FLOOR VENT ALGORITHM

INTRODUCTION

An algorithm has been developed to describe the exchange flow through a horizontal vent, such as a hatch in a ship [1]. Until recently, there was no way to fully characterize the flow through a horizontal vent (Figure 1). The Bernoulli equation has historically been used to calculate uni-directional flow through horizontal vents. The Bernoulli equation, which is valid for all vertical vent (i.e., doors and windows) scenarios, states that the mass flow rate through the vent is proportional to the square root of the difference between the gas pressure inside the compartment and the surrounding atmosphere. Use of this equation to calculate horizontal vent flow leads to an anomaly when the difference between the interior and exterior pressure of the compartment reaches zero. The Bernoulli equation predicts no flow which is clearly impossible when the gas above the vent is more dense than the gas inside the compartment. Gravity dictates that the heavier gas change places with the lighter compartment gas and hence an exchange flow must exist.

The validity of this new algorithm was tested by incorporation into a computer model written to simulate a compartment with a fire inside, which is ventilated through a hole in the ceiling. The model predictions were then compared to the experimental results of reduced scale fire tests [2].

MATHEMATICAL MODEL - AN OVERVIEW

The mathematical model was written to simulate a compartment fire ventilated only through an opening in the ceiling. The zone modeling approach, as opposed to field modeling, was used. The latter describes a system using the basic conservation equations of mass, momentum, and energy in partial differential form. This method provides very high resolution and detail but is computationally intensive for even the simplest fire scenarios. A zone model, on the other hand, can reasonably approximate a much more complicated fire scenario and still have a significantly lower computational requirement. The system is divided into zones which are assumed to be of uniform temperature and composition. Mass and energy balances are written around the zones to describe the interactions between them. The system in this particular case was divided

Manuscript approved January 14, 1991.

into a total of seven zones: the liquid fuel surface, lower flame zone, upper flame zone, enclosure walls, glass viewing plate, ceiling vent, and the interior gaseous medium located between the flame boundaries and the enclosure walls [3]. The system is shown in Figure 2.

Transient phenomena are described through a sequence of time steps. During each time step, there is no accumulation of energy within the lower and upper flame zones, or the fuel surface. The change in mass and energy of the interior gaseous medium is assumed to be constant. Mass and energy balances, along with the equation of state, provide five non-linear algebraic equations which are simultaneously solved for: mass loss rate, lower flame entrainment, upper flame entrainment, interior gas temperature, and net mass out of the compartment. One dimensional unsteady state heat conduction with convection boundary conditions describes the heat transfer through the compartment walls. Numerical methods are used to solve the resulting differential equations for the interior and exterior wall temperatures. The equations and relevant assumptions, which describe the individual zones and their interactions with each other at any given time step, will be explained in more detail in the following sections.

Fuel Source Zone

The liquid fuel is contained in a circular fuel pan and the fuel surface is assumed to remain level with the rim of the pan. Lip exposure is known to affect the burning rate of a liquid pan fire [4]. The temperature of the fuel surface is taken to be equal to the normal boiling point of the liquid fuel and there is no conduction through the fuel or fuel pan [5]. The mass loss rate can then be calculated using the following steady state conservation of energy equation written around the liquid fuel surface:

$$\dot{m}_v C_{liq}(T_s - T_{liq}) + \dot{m}_v \Delta H_v = A_s h_s (T_{lf} - T_s) - \dot{Q}_{r,s}$$

The amount of energy needed to raise the temperature of the fuel to its boiling point, and then to vaporize it, is equal to the convective energy supplied to the fuel surface from the flame and the net radiant energy from the surrounding zones. The specific heat of the liquid fuel is assumed to remain constant.

Flame Zones

The division of the visible flame into an upper zone and a lower zone is adopted from the work of Steward, Fang, Heskestad, Delichatsios and McCaffrey [6-11]. There is fairly good agreement between the various correlations with respect to flame height and temperature. There is, however, a large variation in mass entrainment predictions using the available correlations [12]. Due to this lack of consensus, flame height and temperature are determined using McCaffrey's correlations [11] and an "effective" mass entrainment is calculated based on an energy balance around the flame zones.

The lower flame zone is the continuous region located directly above the fuel surface and is characterized by a constant centerline temperature. The upper flame zone is intermittent in nature. It is the pulsating portion of the flame which raises periodically from the continuous zone at a consistent frequency. The centerline temperature in this upper flame zone decreases with height above the fuel surface as the entrained air cools the product gases.

It is assumed that most of the combustion is occurring in the lower flame zone. McCaffrey found that the energy generated in the intermittent regime is equal to the depletion of energy through radiation [11]. Figures 3 through 5 clearly show that the net radiant heat loss from the upper flame zone is a fraction of the heat generated in the lower flame zone due to combustion for all cases of interest.

The steady state conservation of energy equation as applied to the lower and upper flame zones are as follows:

Lower Flame Zone

$$\dot{m}_v C_v T_s + \dot{m}_{g,1f} C_g T_g + \dot{m}_v \Delta H_c = (\dot{m}_{g,1f}+\dot{m}_v) C_{1f} T_{1f} + A_s h_s (T_{1f}-T_s) + \dot{Q}_{r,1f}$$

The enthalpy of the vaporized fuel and the entrained air, and the energy from the combustion of the fuel must equal the enthalpy of the lower flame zone products, the energy convected to the fuel surface, and the net radiant heat loss from the lower flame zone.

Upper Flame Zone

$$(\dot{m}_{g,1f}+\dot{m}_v) C_{1f} T_{1f} + \dot{m}_{g,uf} C_g T_g = (\dot{m}_{g,1f}+\dot{m}_{g,uf}+\dot{m}_v) C_{uf} T_{top} + \dot{Q}_{r,uf}$$

The enthalpy of the lower flame products and the entrained air into the upper flame zone must equal the upper flame zone products and the net radiant heat loss from the upper flame zone.

The gaseous specific heats are assumed to be constant and equal for the air, fuel, and combustion products leaving the visible flame.

The products leave the respective zones at a temperature based on an assumed squared Gaussian form for the radial variation of the temperature [10,11].

Interior Gas Medium

As the temperature of the gas within the enclosure increases, there must be a net loss of mass through the vent during each time step. This quantity can be determined by assuming that the gas within the enclosure is a perfect gas and applying the equation of state.

$$PV = \left(\frac{m_g}{M_g}\right) RT_g$$

Once sufficient mass loss has occurred, the pressure difference across the vent becomes zero. An instability is created due to the heavier gas above the less dense enclosure gas. An exchange flow occurs which is calculated using the algorithms described in reference 1.

$$\dot{V} = 0.10\,[2gA_o^{2.5}(\rho_{amb}-\rho_g)/(\rho_g+\rho_{amb})]^{0.5}$$

The total mass out of the enclosure is then calculated by summing the appropriate mass flow rates.

$$m_{out} = m_{in} + m_{out,net}$$

The rate of energy change during each time step is assumed to be constant and can be described by the following equation:

$$\dot{E}_g = (\dot{m}_{g,lf}+\dot{m}_{g,uf}+\dot{m}_v)\,C_{uf}T_{top} + \dot{m}_{in}C_{amb}T_{amb} - (\dot{m}_{g,lf}+\dot{m}_{g,uf}+\dot{m}_{out})\,C_gT_g - \dot{Q}_{r,g}$$

$$- h_{gl}A_{gl}(T_g-T_{amb}) - h_wA_w(T_g-T_w)$$

The rate of energy change is equal to the enthalpy of the flame products and of the air entering the enclosure through the vent minus the enthalpy of the entrained air and of the gas exiting the enclosure through the vent, the net radiant heat loss of the enclosure gas, and the heat convected to the walls and the glass viewing plate.

The temperature of the enclosure gas is determined by:

$$T_g = \frac{E_g}{C_gm_g}$$

where the total energy of the gas is:

$$E_g = E_{g,old} + \dot{E}_g(\Delta t)$$

and the mass of the gas in the chamber is given by:

$$m_g = m_{g,old} + (\dot{m}_v-\dot{m}_{out,net})\,\Delta t$$

The composition of the enclosure gas is recalculated during each time interval by accounting for the production and consumption of gas molecules as well as the molecules entering and exiting through the vent opening.

$$m_{O_2} = m_{O_2,old} - m_{O_2,out} + m_{O_2,in} - m_{O_2,consumed}$$

$$m_{H_2O} = m_{H_2O,old} - m_{H_2O,out} + m_{H_2O,in} + m_{H_2O,produced}$$

$$m_{N_2} = m_{N_2,old} - m_{N_2,out} + m_{N_2,in}$$

$$m_{CO_2} = m_{CO_2,old} - m_{CO_2,out} + m_{CO_2,in} + m_{CO_2,produced}$$

The carbon dioxide and water concentrations are used to calculate the absorption-emission properties of the enclosure gas (described below). The average molecular weight of the enclosure gas is required to calculate the net mass out of the enclosure during each time interval. Analysis of the enclosure gas, on a dry gas basis, shows very little carbon monoxide.

	Mass Fraction
Oxygen	0.14 - 0.23
Carbon Dioxide	0 - 0.08
Carbon Monoxide	0 - 0.002
Nitrogen	balance

The combustion reactions are, therefore, assumed to go to completion, leaving the following chemical species for consideration: nitrogen, oxygen, carbon dioxide, and water.

Enclosure Walls

The enclosure in this model is comprised of the walls, floor, and ceiling. Energy is transferred to the interior enclosure via radiation and convection. One dimensional unsteady state conduction with convection boundary conditions describes the heat flow through the enclosure and to the surrounding atmosphere. The equations are solved numerically using an explicit forward differencing technique [13]. The time and distance increments were chosen based on stability and convergence criteria as well as optimization of computation time versus solution accuracy.

RADIANT HEAT TRANSFER EQUATIONS

Analysis of the net radiant heat exchange between the zones is by the net radiation method [14]. The surface radiosities (enclosure and fuel surface) are first determined by:

$$J_i = (1-\epsilon_i)\sum F_{i-j}J_j + \epsilon_i e_{b_i}$$

These are then used to calculate the net radiant heat loss for each surface:

$$\dot{Q}_{ri} = (J_i - G_i) A_i$$

and each gas:

$$\dot{Q}_{rg} = \sum A_i \varepsilon_g (e_{bg} - J_i)$$

Specifically,

Fuel Surface:

$$\dot{Q}_{r,s} = (J_s - G_s) A_s$$

where:

$$J_s = \varepsilon_s e_{bs} + (1-\varepsilon_s) G_s,$$

and

$$G_s = \tau_g \tau_{lf} J_w (1-F_{si}) + \tau_{lf} \varepsilon_g e_{bg} (1-F_{si}) + \varepsilon_{lf} e_{blf} + \tau_g \tau_{lf} \tau_{uf} J_w F_{si} (1-F_{fo})$$

$$+ \tau_{lf} \varepsilon_g e_{bg} \tau_{uf} F_{si} + \varepsilon_{uf} e_{buf} F_{si} \tau_{lf} + F_{si} \tau_{lf} \tau_{uf} \varepsilon_o e_{bo} F_{fo} \tau_g$$

Interior Wall Surface:

$$\dot{Q}_{r,w} = (J_w - G_w) A_w$$

where:

$$J_w = \varepsilon_w e_{bw} + (1-\varepsilon_w) G_w,$$

and

$$G_w = \epsilon_g e_{bg} + \tau_g J_w \left(1 - \frac{1}{A_w}\left(A_{uf} - A_{uf}F_{fo} + A_{lf} + A_o - F_{fo}A_i\right)\right) + \frac{A_{lf}}{A_w}\tau_g \epsilon_{lf} e_{blf}$$

$$+ \tau_g \tau_{lf} J_s \frac{A_s}{A_w}\left(1 - F_{si}\right) + \tau_g \epsilon_{uf} e_{buf} \frac{A_{uf}}{A_w}\left(1 - F_{fo}\right)$$

$$+ \frac{A_o}{A_w}\left(\epsilon_o e_{bo} \tau_g \left(1 - F_{fo}\frac{A_i}{A_o}\right) + \tau_g \tau_{lf} \tau_{uf} J_s \left(1 - F_{fo}\right)\frac{A_i}{A_w} F_{si}\right.$$

$$+ \tau_{uf} \frac{A_i}{A_w} \epsilon_{lf} e_{blf} \tau_g \left(1 - F_{fo}\right)$$

Lower Flame Zone:

$$\dot{Q}_{r,lf} = \left(A_s + A_{lf} + A_i\right)\epsilon_{lf} e_{blf} - A_s \epsilon_{lf} J_s - A_{lf}\epsilon_{lf}\epsilon_g e_{bg} - A_{lf}\epsilon_{lf}\tau_g J_w$$

$$- A_i \epsilon_{lf} \epsilon_{uf} e_{buf} - A_i \epsilon_{lf} \tau_{uf} \epsilon_g e_{bg} - A_i \epsilon_{lf} \tau_{uf} \tau_g J_w \left(1 - F_{fo}\right) - A_i \epsilon_{lf} \tau_{uf} \epsilon_o e_{bo} F_{fo} \tau_g$$

Upper Flame Zone:

$$\dot{Q}_{r,uf} = \left(A_i + A_{uf}\right)\epsilon_{uf} e_{buf} - A_i \epsilon_{uf} \epsilon_{lf} e_{blf} - A_i \epsilon_{uf} J_s \tau_{lf} F_{si} - A_{uf}\epsilon_{uf}\epsilon_g e_{bg}$$

$$- A_{uf}\epsilon_{uf}\tau_g J_w \left(1 - F_{fo}\right) - A_{uf}\epsilon_{uf}\epsilon_o e_{bo} F_{fo} \tau_g$$

Enclosure Gas:

$$\dot{Q}_{r,g} = (A_w+A_{lf}+A_{uf}+A_o)\,\varepsilon_g e_{bg} - A_w\varepsilon_g J_w - \varepsilon_g A_{lf}\varepsilon_{lf} e_{blf} - \varepsilon_g \varepsilon_{uf} A_{uf} e_u$$

$$- \varepsilon_g A_{lf}\tau_{lf} J_s \frac{A_s}{A_{lf}}(1-F_{si}) - \varepsilon_g A_{uf}\tau_{lf}\tau_{uf} J_s \frac{A_i}{A_{uf}} F_{si} - A_o\varepsilon_o e_{bo}$$

$$- A_{uf}\varepsilon_g \frac{A_i}{A_{uf}}\tau_{uf}\varepsilon_{lf} e_{blf}$$

Initial calculation of the surface radiosities requires knowledge of the view factors between the various surfaces and gas boundaries. The view factor for the fuel surface to the interface between the lower and upper flame zones must be calculated along with the view factor for the visible flame to the vent opening. The remaining view factors are either zero or unity, or can be derived using the reciprocity theorem or the summation rule for an enclosure.

The view factor configuration for the interface between the two visible flame zones and the fuel surface is represented as two parallel circular disks with centers along the same normal [15]. For the purposes of the radiation calculations, the two zones of the visible flame are depicted as two vertically aligned cylinders. The view factor for the circular vent to the visible flame is, therefore, also determined using the configuration of two parallel circular disks with centers along the same normal.

The view factor between the square vent and visible flame should ideally be calculated using a circle and a rectangle configuration. Since there is no analytical solution for this particular geometry [16], the "corners" of the square were ignored and the previously mentioned circle to circle geometry was assumed. This translates into an error in the view factor value of less than four percent for a typical model simulation.

The heights of the cylinders were calculated using McCaffrey's correlation [10,11]:

$$z_{uf} = 0.2(\dot{m}_v \Delta H_c)^{0.4}$$

$$z_{lf} = 0.08(\dot{m}_v \Delta H_c)^{0.4}$$

Values for the surface and gas emissivities are required to perform the radiation calculations. The walls, fuel surface, and glass viewing plate are assumed to be gray and opaque. Their emissivities are constant and equal to 0.9, 0.42, and 0.9, respectively [3,13]. The gases within the two visible flame zones and the enclosure are gray and transmitting. The emissivity of the gases within the visible flame zones are determined during each time interval using the mean beam length approximation:

$$e_g = 1 - e^{-aL_e}$$

where

$$L_e = 3.6\left(\frac{Volume}{Area}\right)$$

and "a" is the absorption coefficient.

Leckner's approximation [17] is used to calculate the emissivity of the enclosure gas. The emissivity is a function of the partial pressure of H_2O and CO_2 within the enclosure. The mean beam length, the temperature, and pressure of the gas are also used to calculate the emissivity of the gas during each time interval.

EXPERIMENTAL STUDY

Reduced scale fire tests were conducted to obtain results which were then compared to the model's predictions. The test apparatus consisted of a 0.43 m (17 in.) cube with 0.0254 m (1 in.) Kaowool walls and 0.0381 m (1.5 in.) Marinite floor and ceiling. There were several ceiling boards, each with a different size circular opening, which allowed for variation of the vent size. A 0.216 m (8.5 in.) square pyrex plate was positioned on one wall for viewing the compartment interior. Ethanol was burned in a 0.11 m (4.25 in.) fuel pan. The fuel supply system was designed to maintain the fuel surface flush

with the top of the pan rim, thereby eliminating an exposed rim which is known to affect the burning rate. An experimental measurement of the mass loss rate was determined from a load cell located beneath the fuel supply reservoir. Nineteen thermocouples were located throughout the compartment. Interior gas temperatures were measured at various levels along with the interior and exterior wall temperatures. An interior gas analysis gave oxygen, carbon monoxide, and carbon dioxide concentrations. Two tests were run at each of the following vent diameters: 0.1016 m (4 in.), 0.127 m (5 in.), and 0.1524 m (6 in.). Experiments were also conducted in the "no vent" (top completely closed) and "maximum vent" (top completely open) configuration. The 0.1016 m (4 in.) opening was not large enough to sustain burning so the fire self-extinguished after a few minutes. Further details of the experimental set-up and procedure are described in reference 2.

RESULTS

The experimental results for the 0.127 m (5 in.) vent experiments (exp 14 and 19) are shown along with the model predictions in Figures 6 through 11. The 0.1524 m (6 in.) experiments (exp 15 and 18) and open top experiments (exp 16 and 17) are depicted in Figures 12 through 17, and Figures 18 through 23, respectively. The Figures are time plots of: mass loss rate, oxygen concentration, carbon dioxide concentration, interior gas temperature, interior wall temperature, and exterior wall temperature. In general, there was very good agreement between the model predictions and the experimental results. There was also very good experimental reproducibility as evidenced by the plots of mass loss rate and interior gas temperature. Note, one of the assumptions made in the model is that the interior is well mixed, i.e. the interior gas is one zone. In reality, there was stratification with respect to temperature. There was also stratification with respect to oxygen and carbon dioxide concentration as is evidenced in the Figures 7, 8, 13, 14, 19, and 20. The gas sampling point was near the top of the compartment in experiments 14, 15, and 16, and near the bottom of the compartment in experiments 17, 18, and 19. The wall temperatures were measured only in experiments 17, 18, and 19.

The excessive amount of scatter in the fuel mass loss rate measurement makes it difficult to distinguish a rate change with time for any of the experiments, although the model predicted a slight increase for both the 0.127 m (5 in.) and 0.1524 m (6 in.). The model did, however, correctly predict that higher burning rates corresponded to larger vent openings and the predicted rates were within the scatter of the measurement. The 0.1524 m (6 in.) experiments showed an approximate 0.3 kg/hr burning rate, whereas the 0.127 m (5 in.) demonstrated about 0.2 kg/hr. The mass loss rate in the open top experiments averaged

0.5 kg/hr which, according to literature predictions [18], is equivalent to an open fire burning rate.

The average oxygen concentration decreased with time in both the 0.1524 m (6 in.) and the 0.127 m (5 in.) experiments as predicted by the model. The model predicted a higher concentration of oxygen for the 0.1524 m (6 in.) configuration relative to the 0.127 m (5 in.). This was also verified experimentally. The model slightly under predicted the oxygen concentration for the two smaller vent openings. The model predictions for the open top configuration, however, were very close to experimental results which remained slightly below normal atmospheric conditions for the entire test.

As the oxygen concentration decreased, the carbon dioxide concentration increased, in both the 0.127 m (5 in.) and 0.1524 m (6 in.) experiments and corresponding model predictions. The increases and their relative magnitudes were correctly predicted by the model. Again, the open top experiments were only slightly elevated above normal atmospheric concentrations for the entire test.

The average interior gas temperatures at the end of the test period in the 0.1524 m (6 in.) and 0.127 m (5 in.) experiments were significantly higher than the temperatures reached in the open top experiments, i.e. 600 K versus 400 K. It appears that the smaller vent openings, while reducing the burning rates, also served to restrict the loss of energy through the hole. In addition, more ceiling surface area translated into more radiation feedback. This rate of temperature increase was also seen in the model results, although somewhat underpredicted. The interior wall temperatures corresponded to the interior gas temperatures both experimentally and in the model predictions. The exterior wall temperatures were similar in all three experiments as predicted by the model.

The conditions within the compartment apparently had opposing influences on the behavior of the fire. The fires in the 0.127 m (5 in.) and 0.1524 m (6 in.) vent opening experiments burned significantly slower than the fires in the open top experiments even though their environment was much hotter. The offsetting condition was, of course, the vitiated enclosure gas. Another example is given by the result that the open top experiments showed a mass loss rate comparable to the burning rate of a fire in the open. The enhancement expected due to the radiation feedback from the walls was not apparent even though the interior gas temperature was elevated compared to normal atmospheric, i.e. 400 K versus 300 K. Again, the experimental results showed that the oxygen concentration was slightly lower than normal atmospheric.

SUMMARY

The validity of the horizontal vent algorithm was verified by incorporation into a mathematical model and then demonstrating that the model predictions were comparable to experimental results. The intent was not to accurately model a fire burning in a vitiated environment - a complicated and still largely undefined phenomenon. The intent was rather to show that, for a given burning rate, the algorithm was able to predict from the area of the vent opening and the density of the interior gas (and thereby, composition and temperature of the gas), a mass flow which correctly accounted for the fire's oxygen consumption and energy output. The horizontal vent algorithm accomplished this on a small scale basis. To further test and confirm this algorithm, a similar comparison should be made on a larger scale.

REFERENCES

1. Cooper, L.Y., "Calculation of the Flow Through a Horizontal Ceiling/Floor Vent", National Institute of Standards and Technology, NISTIR 4402 (1989).

2. Tu, K.M., "An Experimental Study of Top Vented Compartment Fire", National Institute of Standards and Technology, to be published.

3. Tatem, P.A., Williams, F.W., Ndubizu, C.C., and Ramaker, D.E., "Influence of Complete Enclosure on Liquid Pool Fires", Combustion Science and Technology 45:185 (1986).

4. Santo, G., and Tamanini, F., "Influence of Oxygen Depletion on the Radiative Properties of PMMA Flames", Eighteenth Symposium (Int.) on Combustion, The Combustion Institute (1981), p. 619.

5. Drysdale, D., An Introduction to Fire Dynamics, John Wiley and Sons, New York (1985).

6. Steward, F.R., "Prediction of the Height of Turbulent Diffusion Buoyant Flames", Combustion Science and Technology 2:203 (1970).

7. Fang, J.B., "Analysis of the Behavior of a Freely Burning Fire in a Quiescent Atmosphere", National Bureau of Standards, NBSIR 73-115 (1973).

8. Heskestad, G., "Engineering Relations for Fire Plumes", Fire Safety Journal 7:25 (1984).

9. Delichatsios, M.A., "Air Entrainment into Buoyant Jet Flames and Pool Fires", SFPE Handbook of Fire Protection Engineering (1988).

10. McCaffrey, B.J., "Purely Buoyant Diffusion Flames: Some Experimental Results", National Bureau of Standards, NBSIR 79-1910 (1979).

11. McCaffrey, B.J., "Momentum Implications for Buoyant Diffusion Flames", Combustion and Flame 52:149 (1983).

12. Beyler, C.L., "Fire Plumes and Ceiling Jets", Fire Safety Journal 11:53 (1986).

13. Holman, J.P., Heat Transfer, McGraw-Hill Book Company, New York (1976).

14. Eckert, E.R.G., and Drake, R.M., Analysis of Heat and Mass Transfer, McGraw-Hill Book Company, New York (1972).

15. Siegel, R., and Howell, J.R., Thermal Radiation Heat Transfer, McGraw-Hill Book Company, New York (1972).

16. Tripp, W., Hwang, C., Crank, R.E., "Radiation Shape Factors for Plane Surfaces and Spheres, Circles or Cylinders", Special Report 16, Kansas State University Bulletin, 46, No 4 (1962).

17. Leckner, B., "Spectral and Total Emissivity of Water Vapor and Carbon Dioxide", Combustion and Flame 19:33 (1972).

18. Babrauskas, V., "Burning Rates", *SFPE Handbook of Fire* Protection Engineering (1988).

NOMENCLATURE

A	surface area
C	specific heat
e_b	black body emissive power
g	acceleration of gravity
G	irradiation (total radiation incident upon a surface per unit time and per unit area)
h	convective heat transfer coefficient
ΔH_c	heat of combustion
ΔH_v	latent heat of vaporization
J	radiosity (total radiation which leaves a surface per unit time and per unit area)
m	mass
$\dot{m}$	mass flow rate
M	molecular weight
$\dot{Q}$	power
R	universal gas constant
P	pressure
T	absolute temperature
Δt	time interval
V	volume
z	height
ρ	density
ϵ	emissivity
τ	transmissivity

View Factors

F_{si}	surface to flame zone interface
F_{fo}	flame to vent opening

Subscripts

amb	ambient
g	interior gas
gl	glass
i	interface between flame zones
lf	lower flame zone
liq	liquid fuel
o	vent opening
old	previous time interval
out	out
r	radiant energy
s	fuel surface
top	top of visible flame
uf	upper flame zone
v	fuel vapor
w	interior wall surface

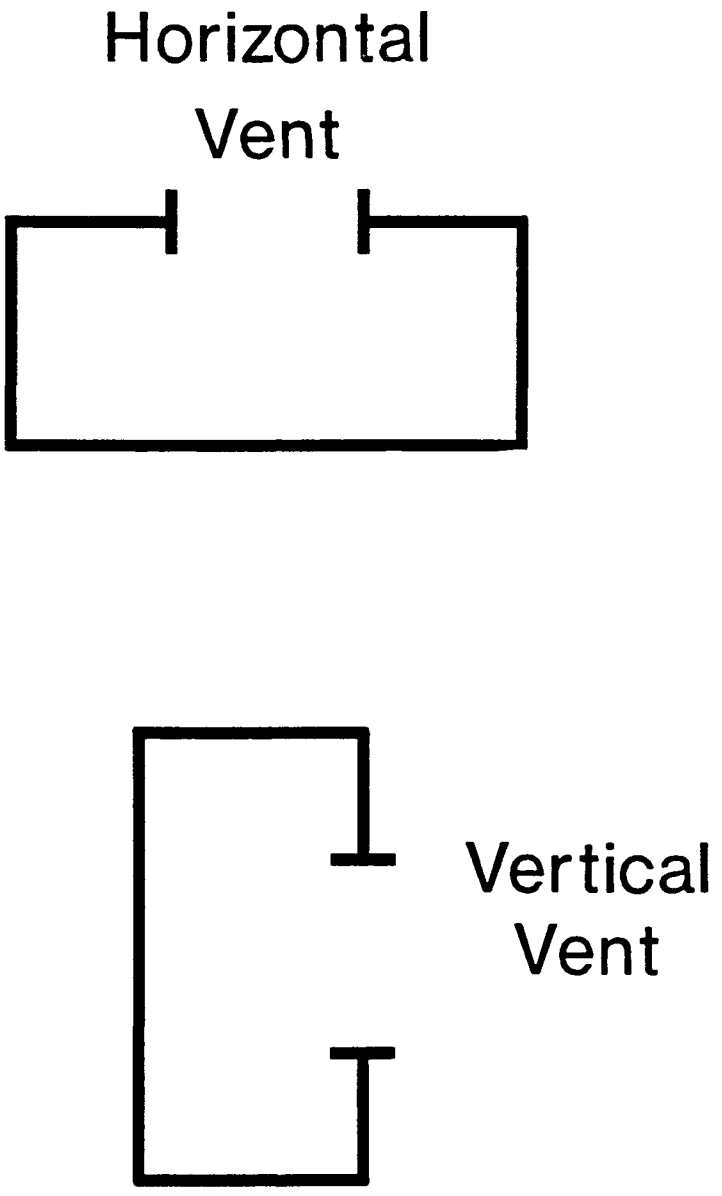

Figure 1. Vent Configuration.

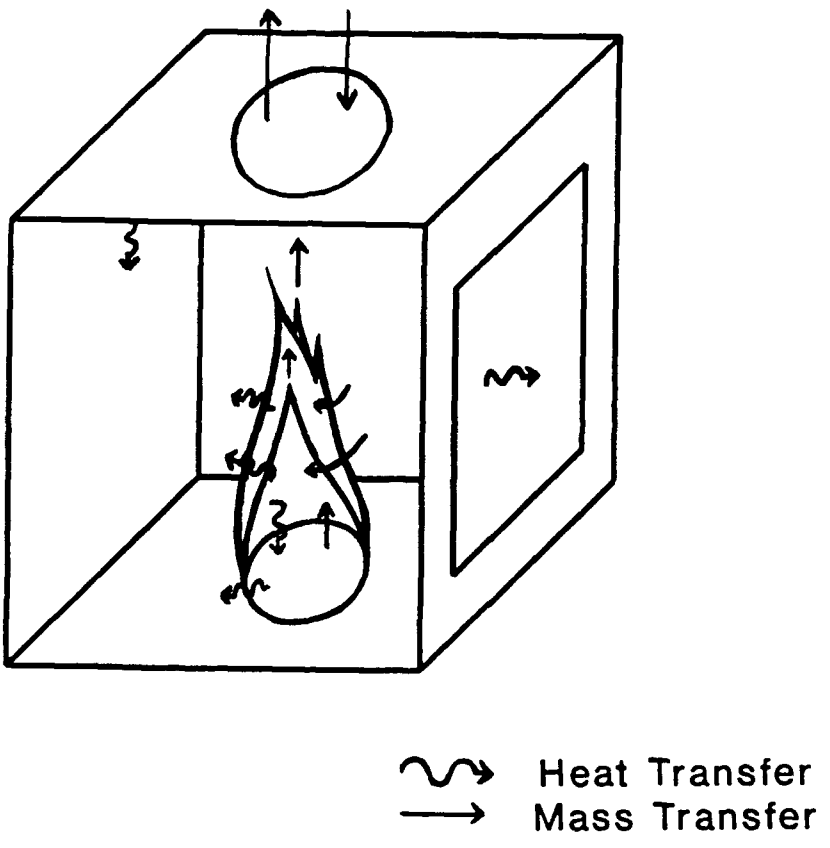

Figure 2. Modeled System.

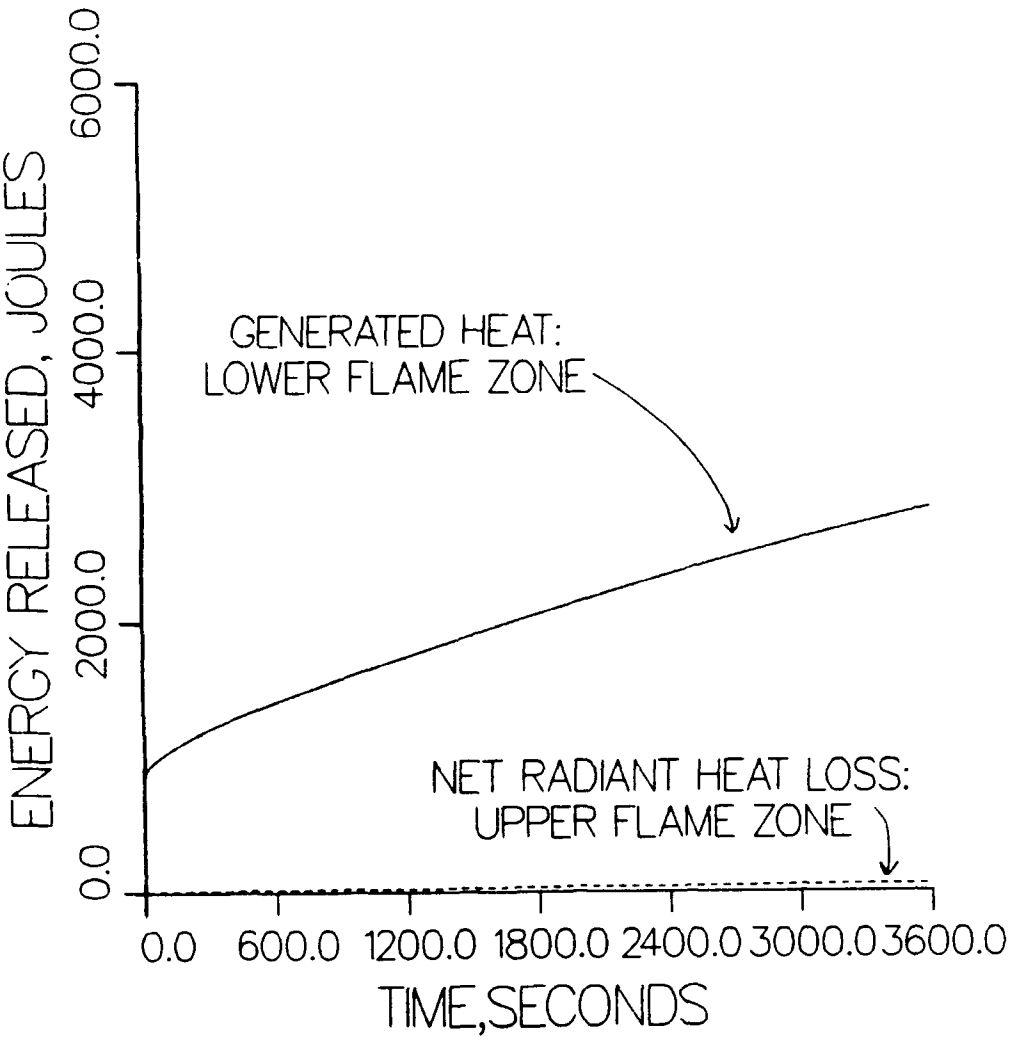

Figure 3. Intermittent flame zone net radiant heat loss vs. heat of combustion in lower flame zone. (0.127 m vent opening)

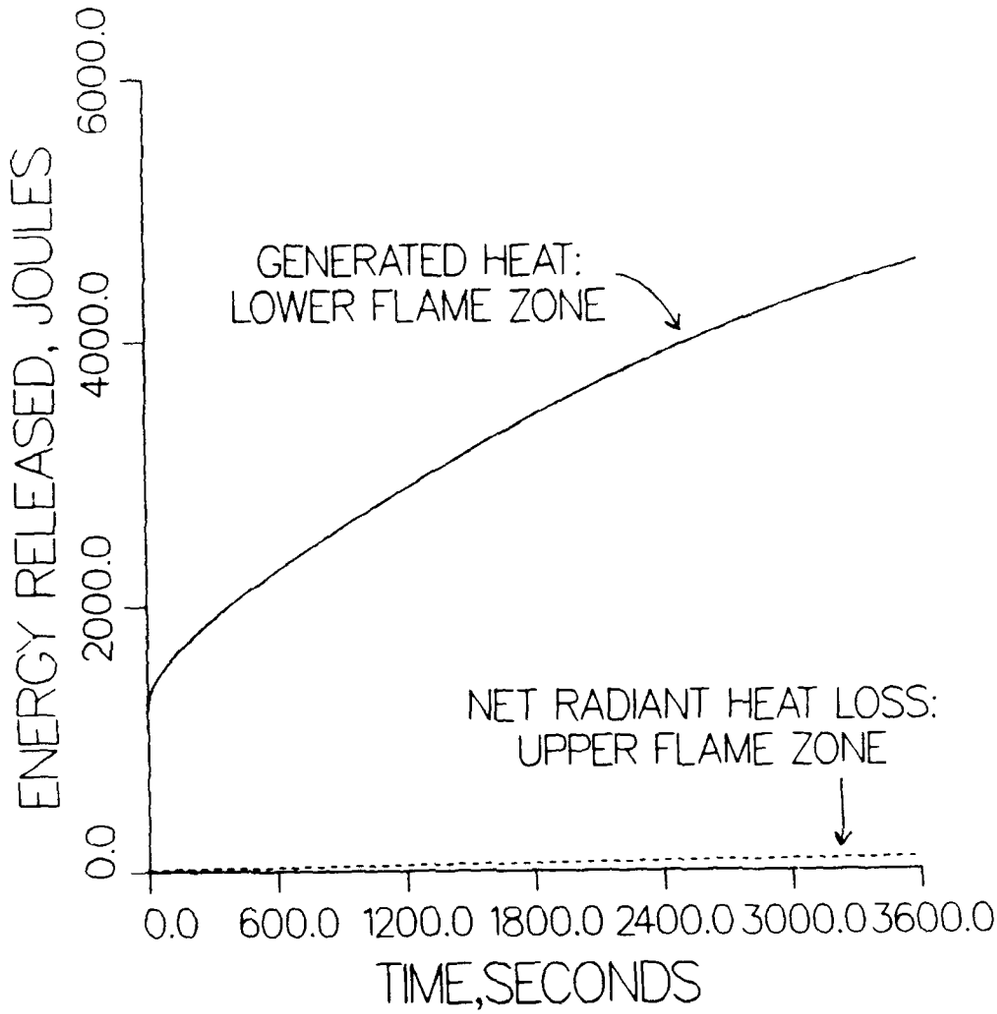

Figure 4. Intermittent flame zone net radiant heat loss vs. heat of combustion in lower flame zone. (0.1524 m vent opening)

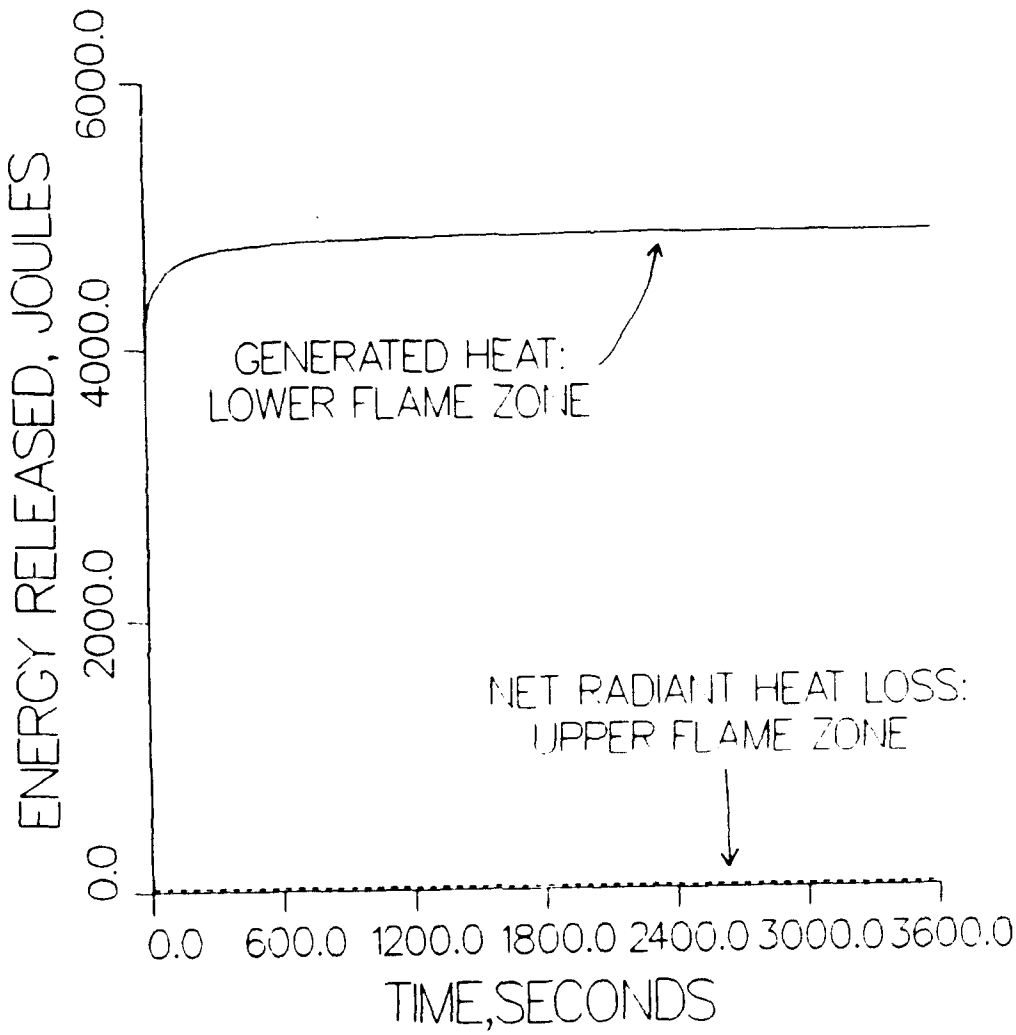

Figure 5. Intermittent flame zone net radiant heat loss vs. heat of combustion in lower flame zone. (open top)

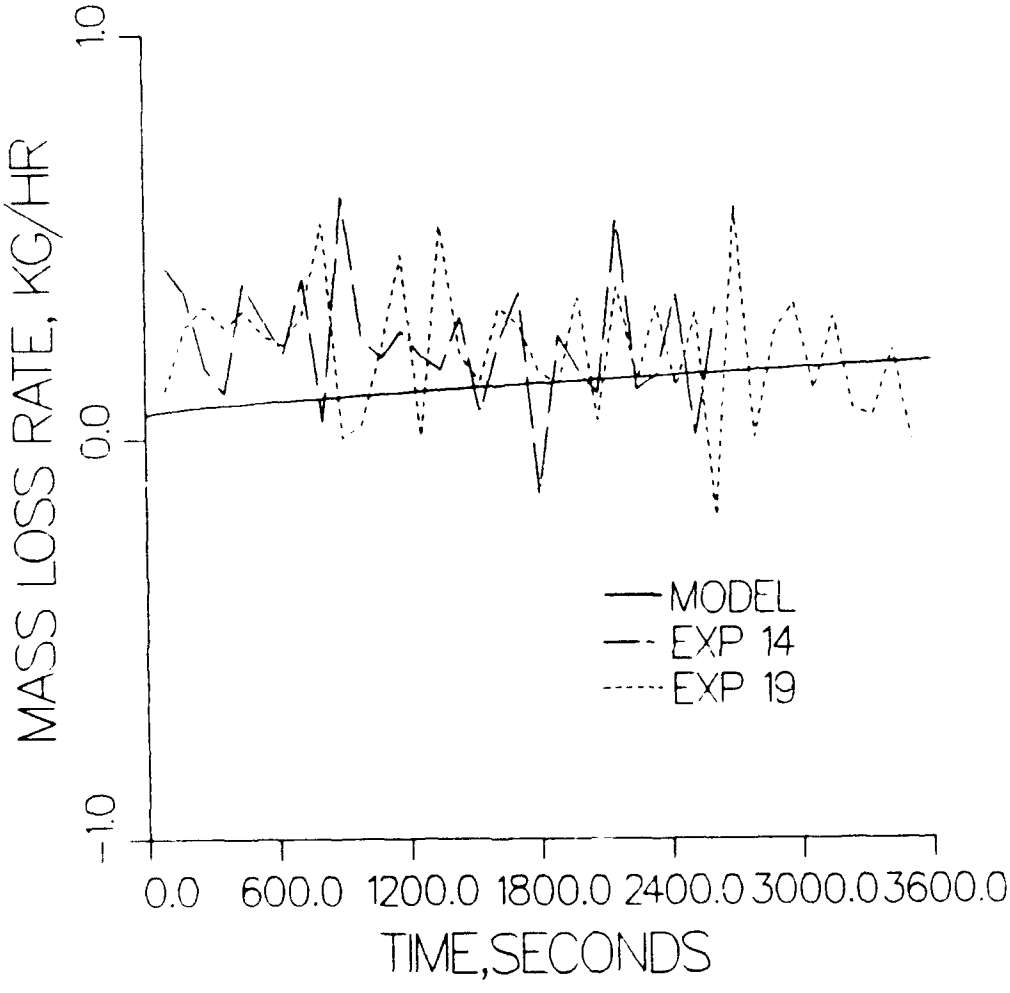

Figure 6. Model predictions versus results from 0.127 m (5 in) vent opening experiments.

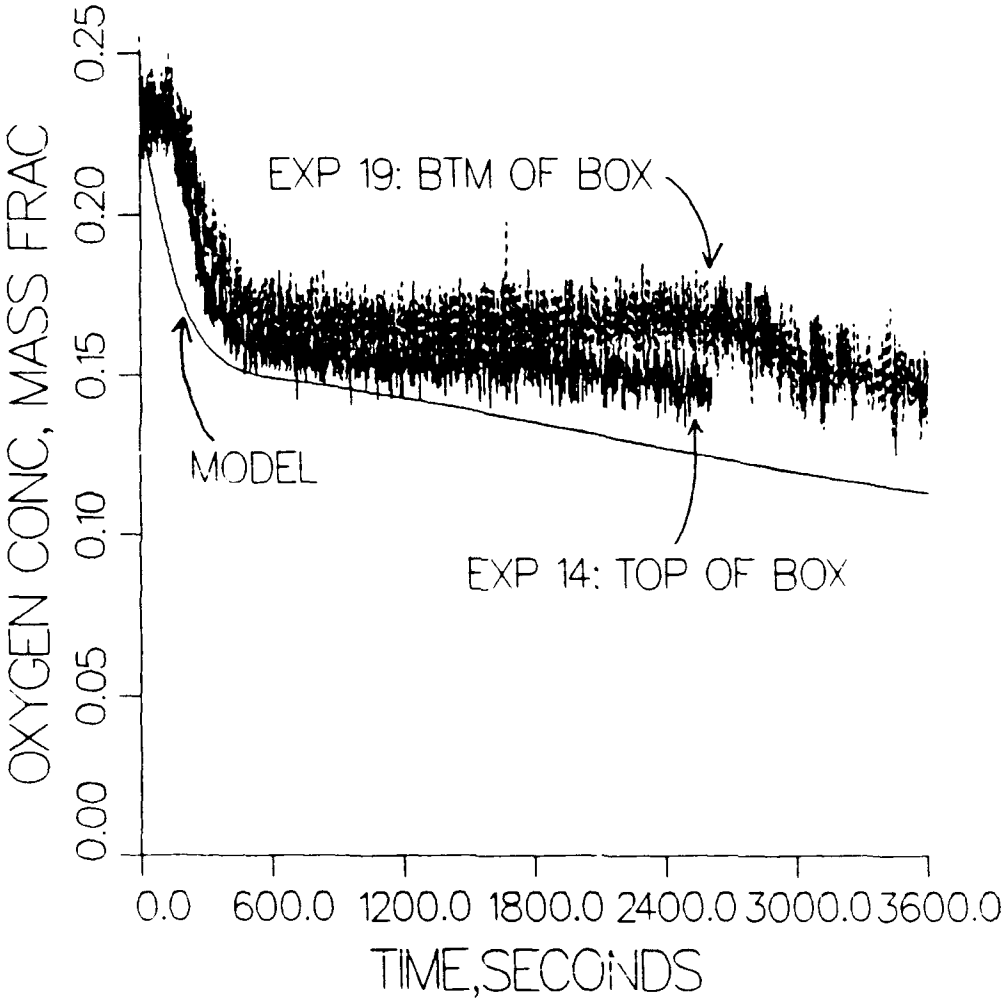

Figure 7. Model predictions versus results from 0.127 m (5 in) vent opening experiments.

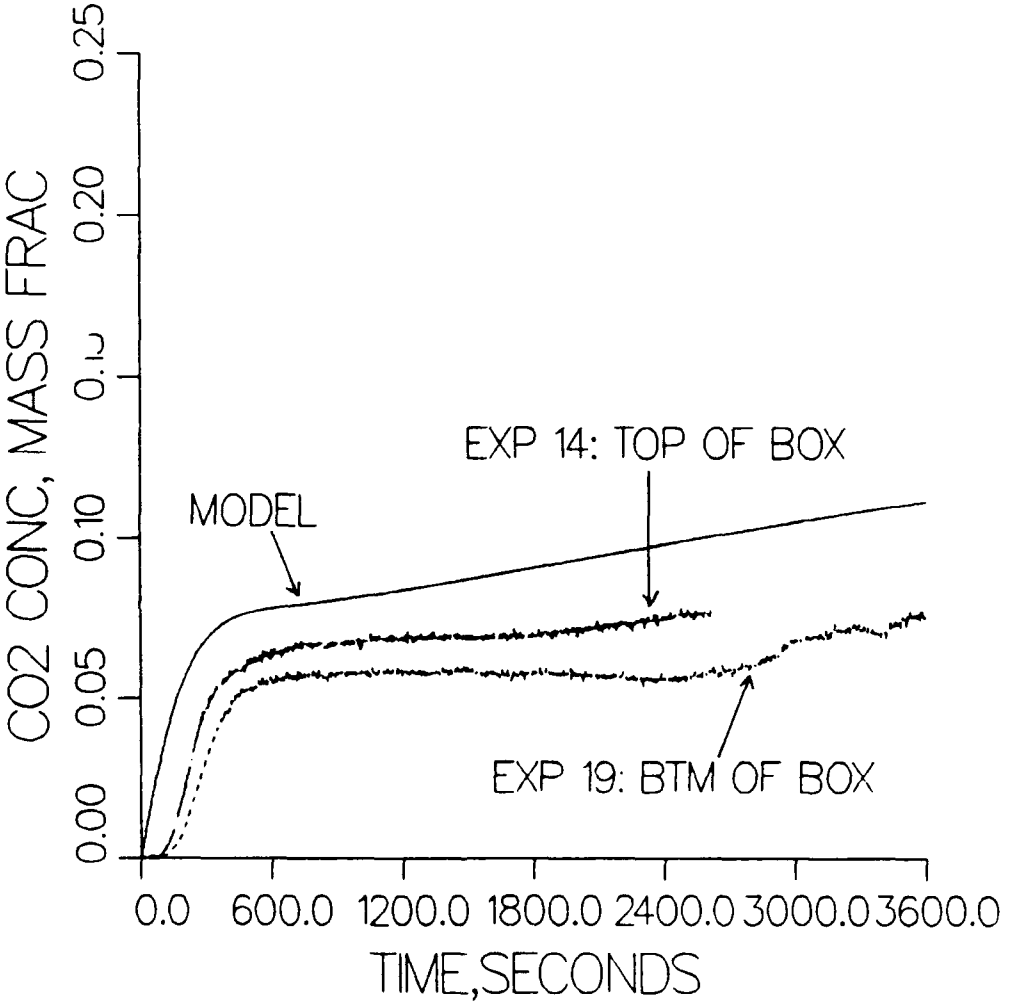

Figure 8. Model predictions versus results from 0.127 m (5 in) vent opening experiments.

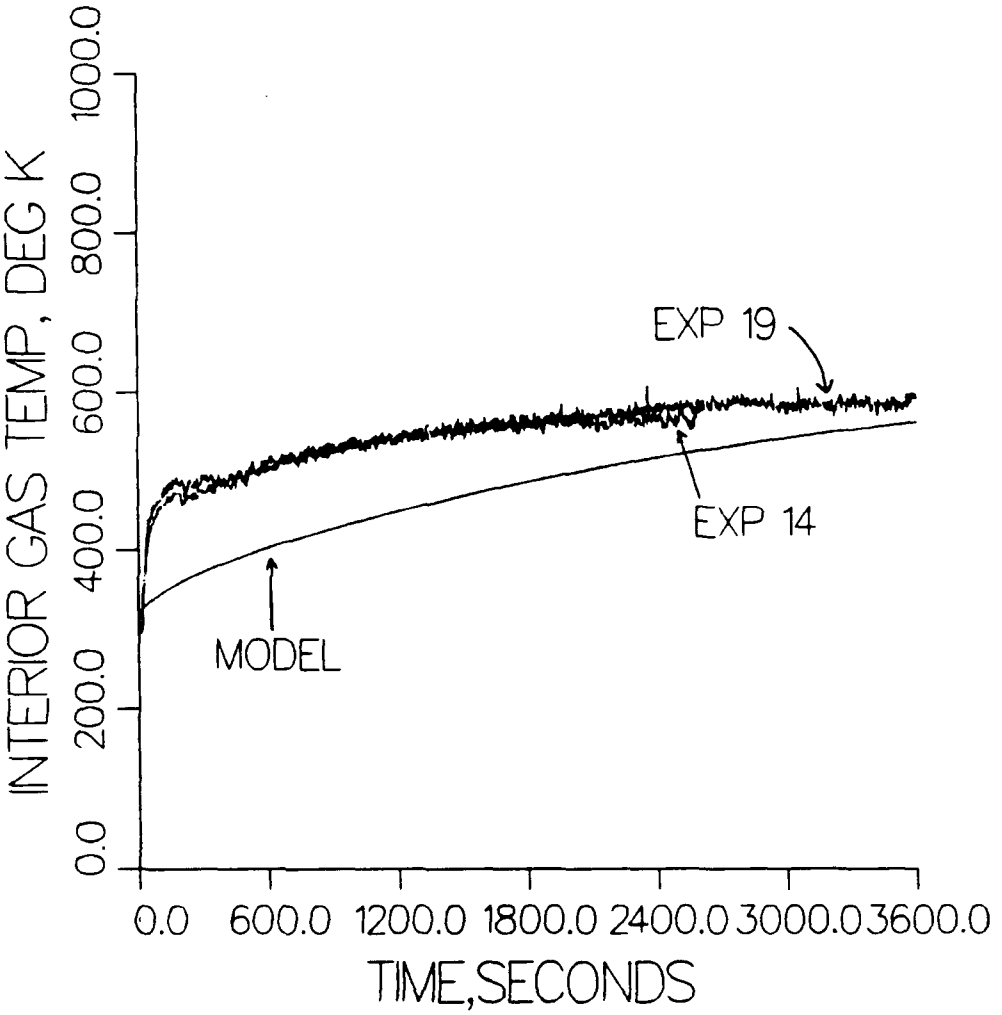

Figure 9. Model predictions versus results from 0.127 m (5 in) vent opening experiments.

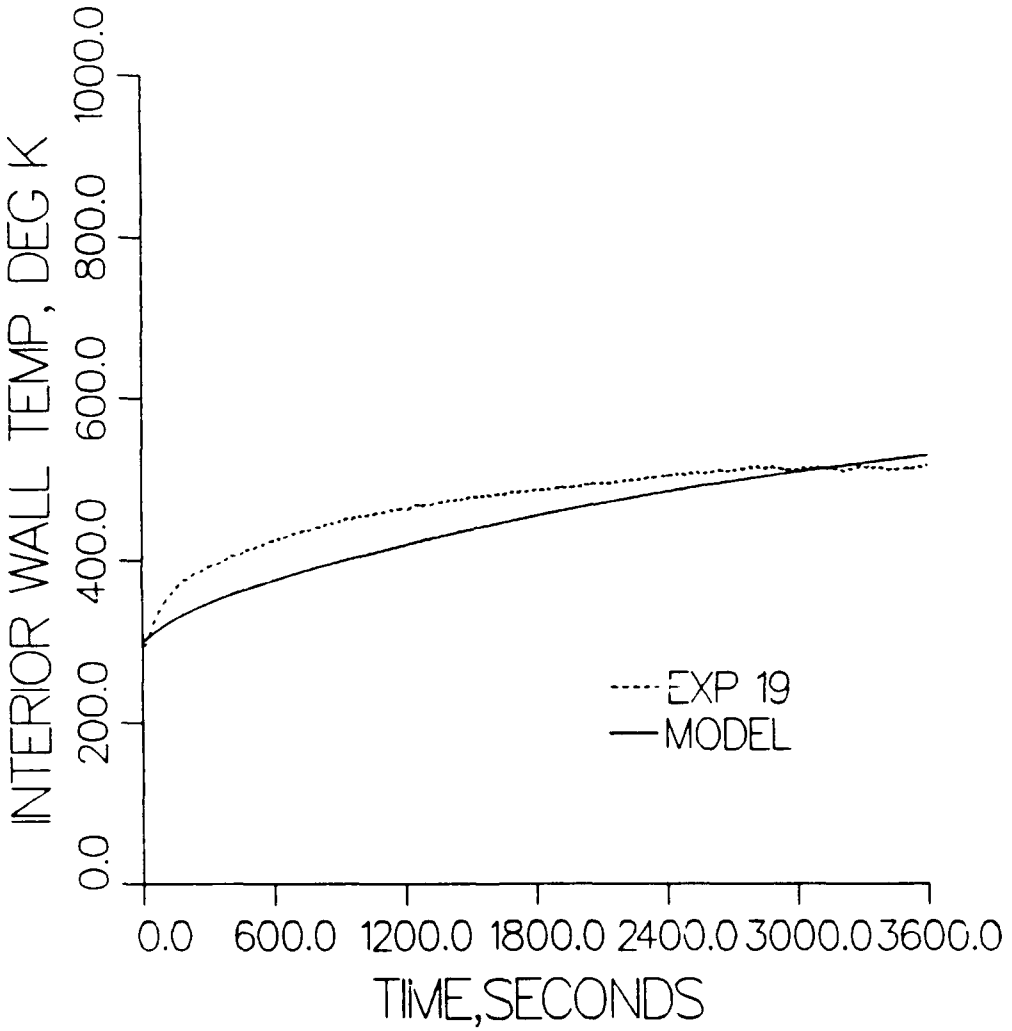

Figure 10. Model predictions versus results from 0.127 m (5 in) vent opening experiments.

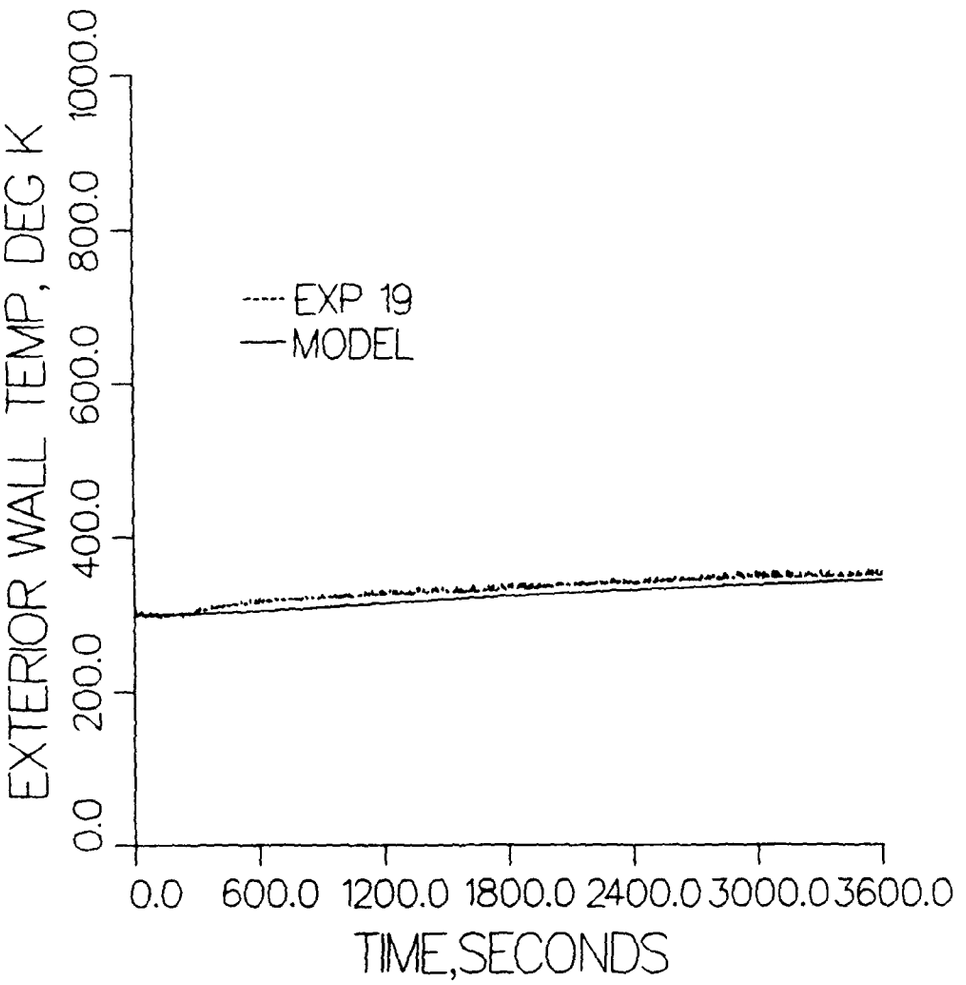

Figure 11. Model predictions versus results from 0.127 m (5 in) vent opening experiments.

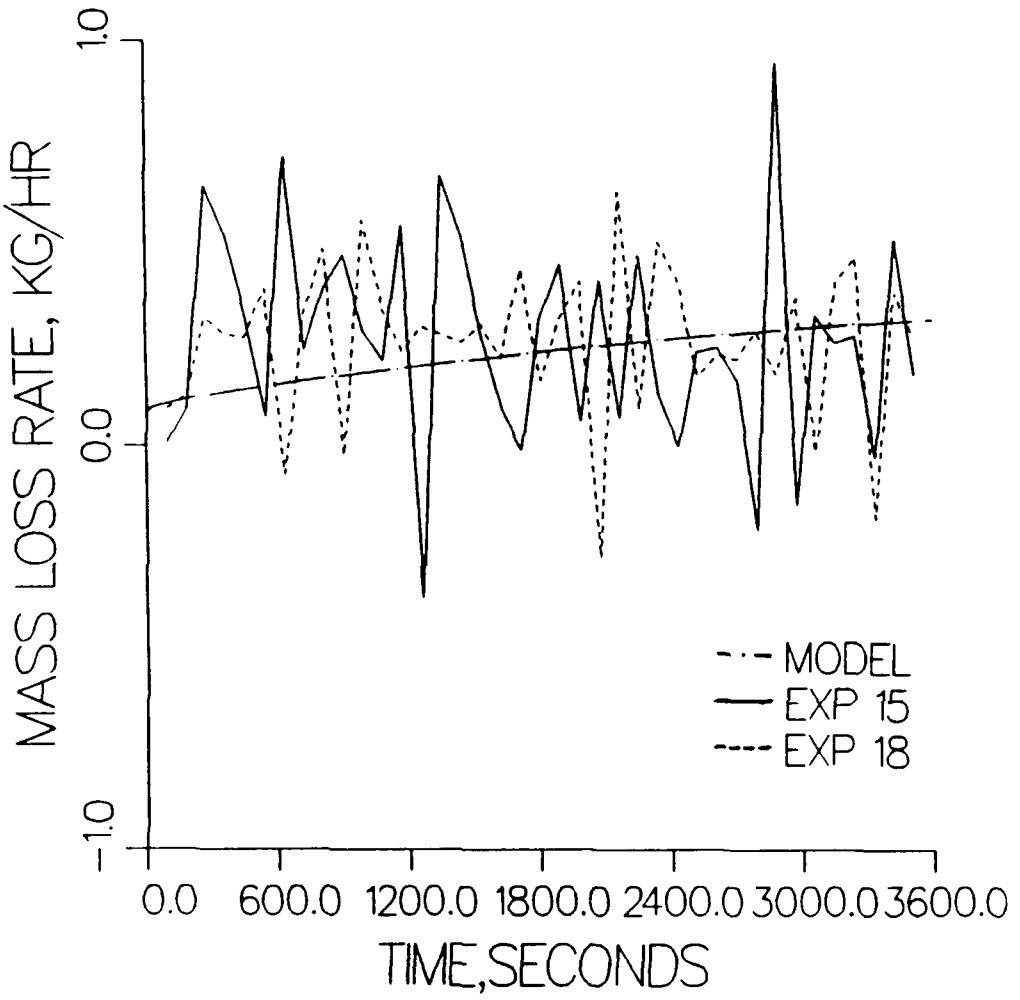

Figure 12. Model predictions versus results from 0.154 m (6 in) vent opening experiments.

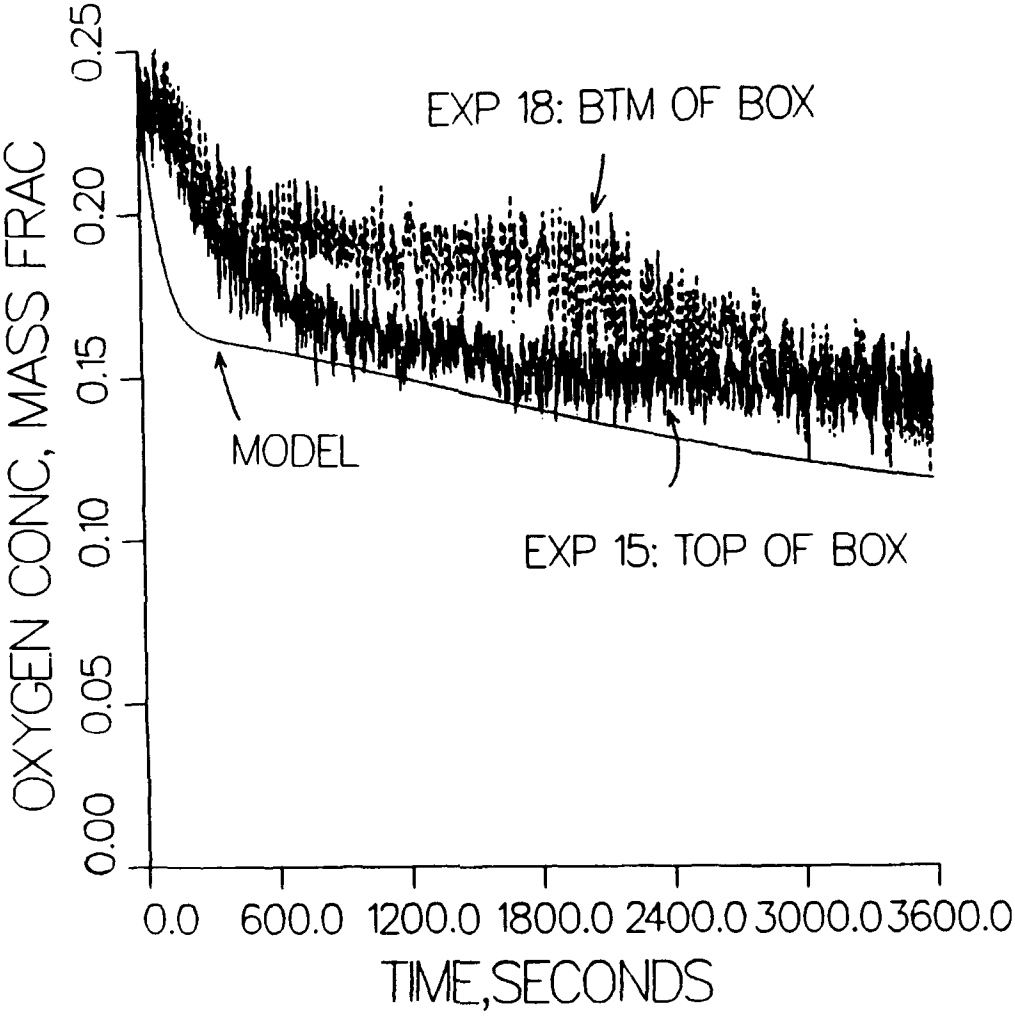

Figure 13. Model predictions versus results from 0.154 m (6 in) vent opening experiments.

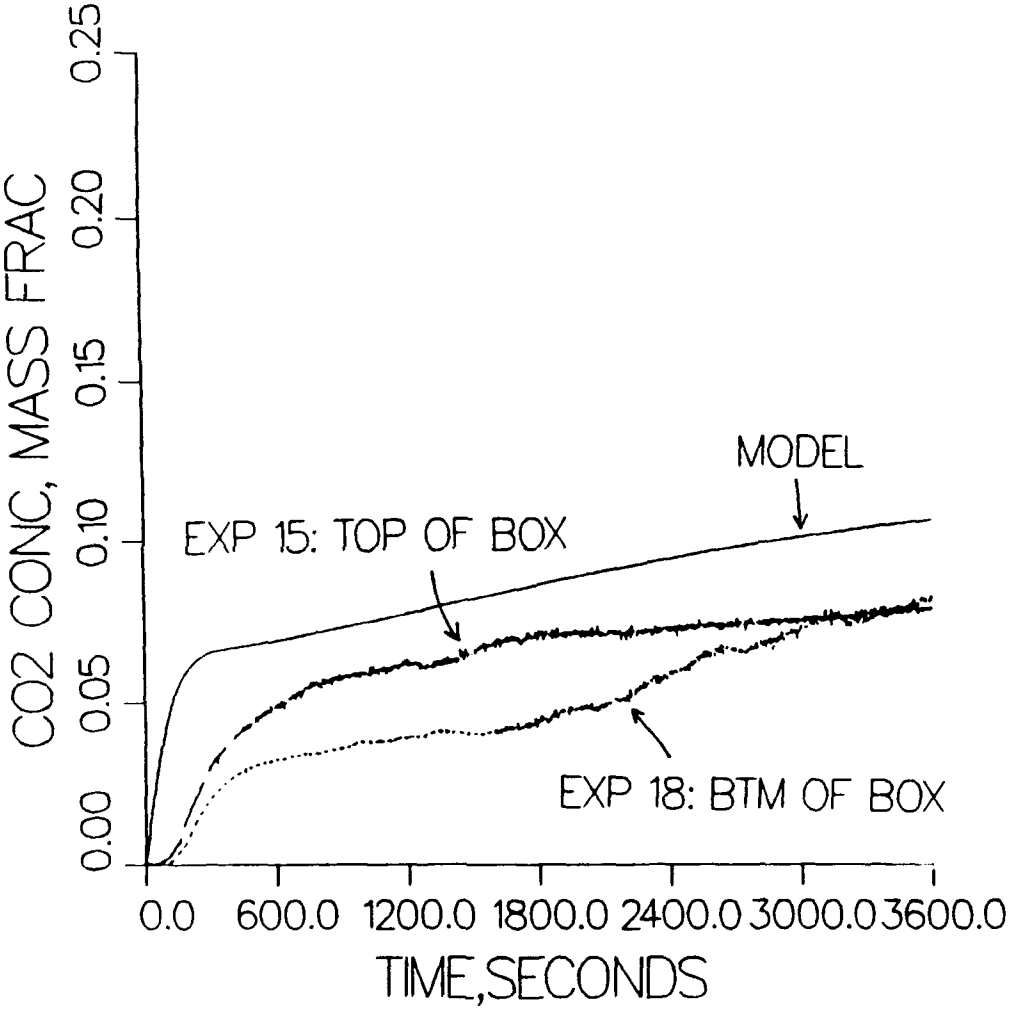

Figure 14. Model predictions versus results from 0.154 m (6 in) vent opening experiments.

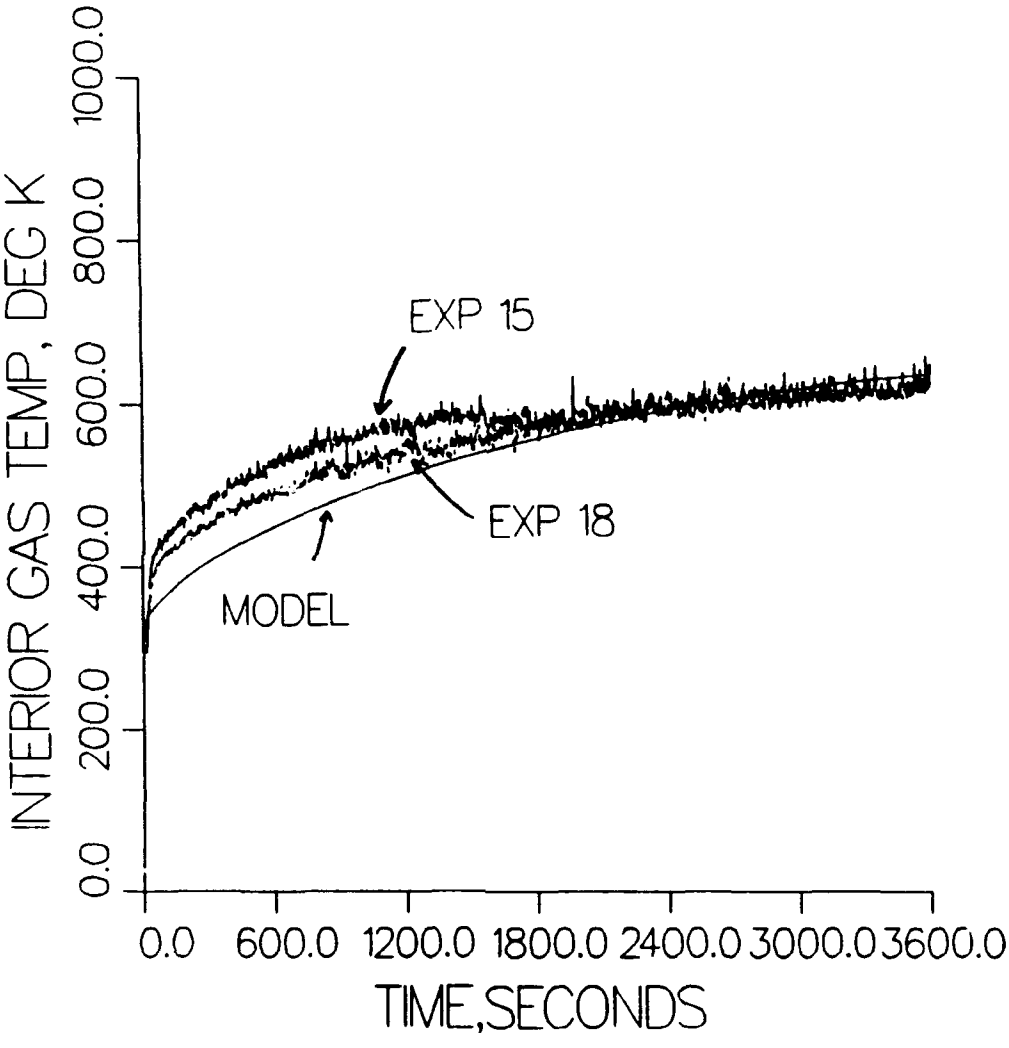

Figure 15. Model predictions versus results from 0.154 m (6 in) vent opening experiments.

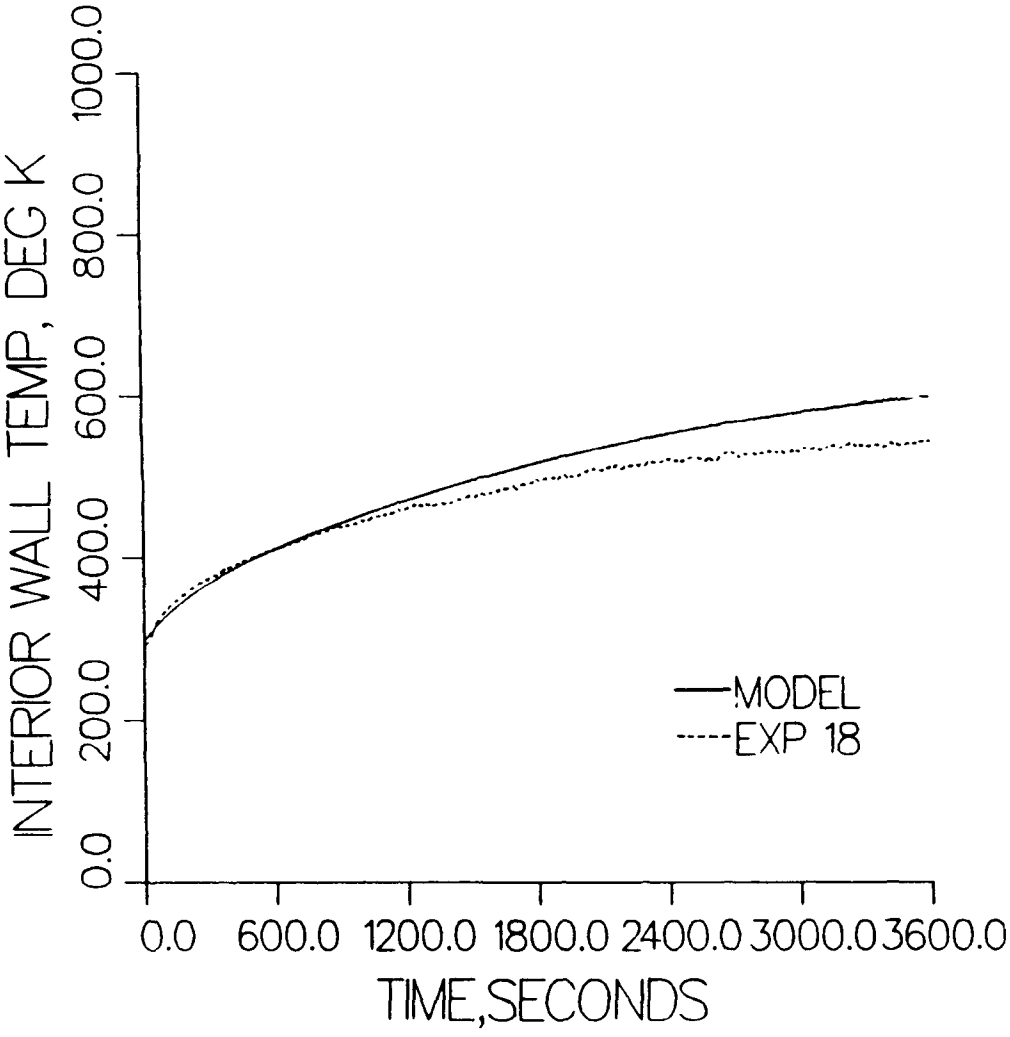

Figure 16. Model predictions versus results from 0.154 m (6 in) vent opening experiments.

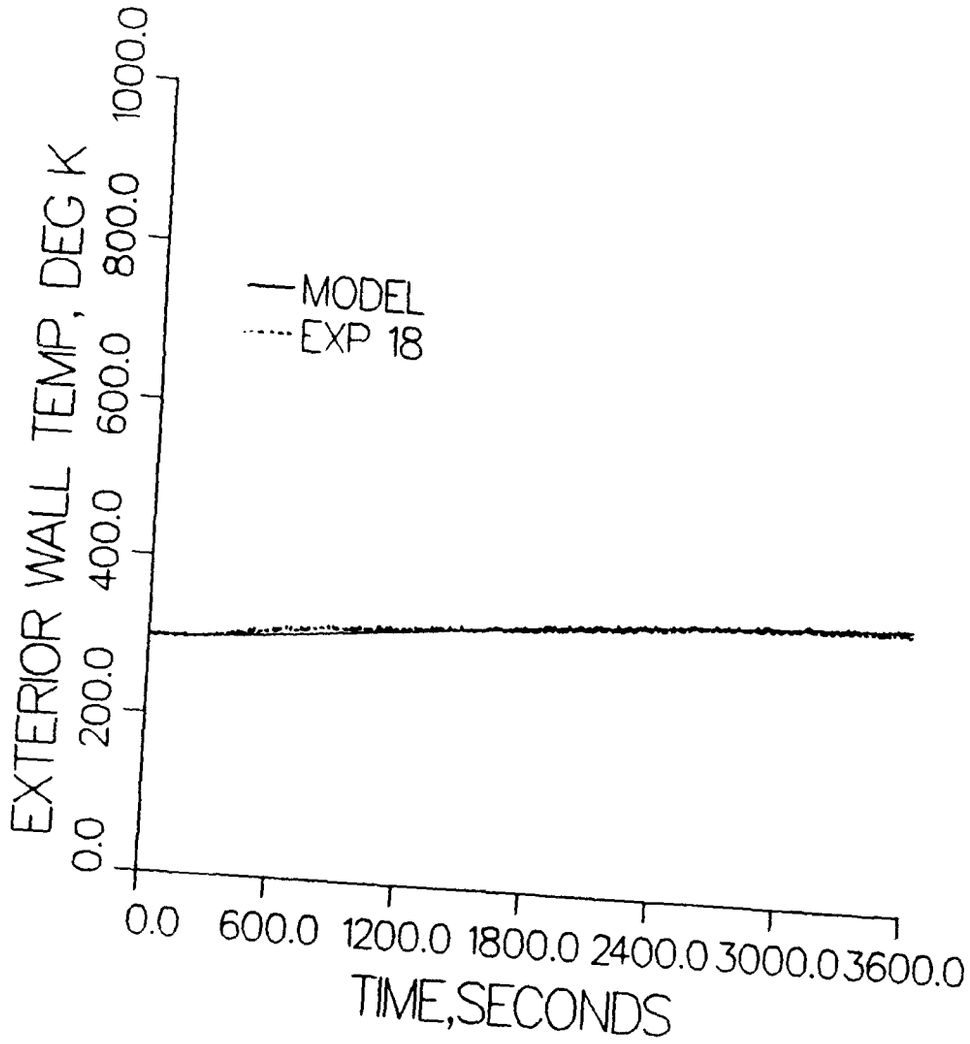

Figure 17. Model predictions versus results from 0.154 m (6 in) vent opening experiments.

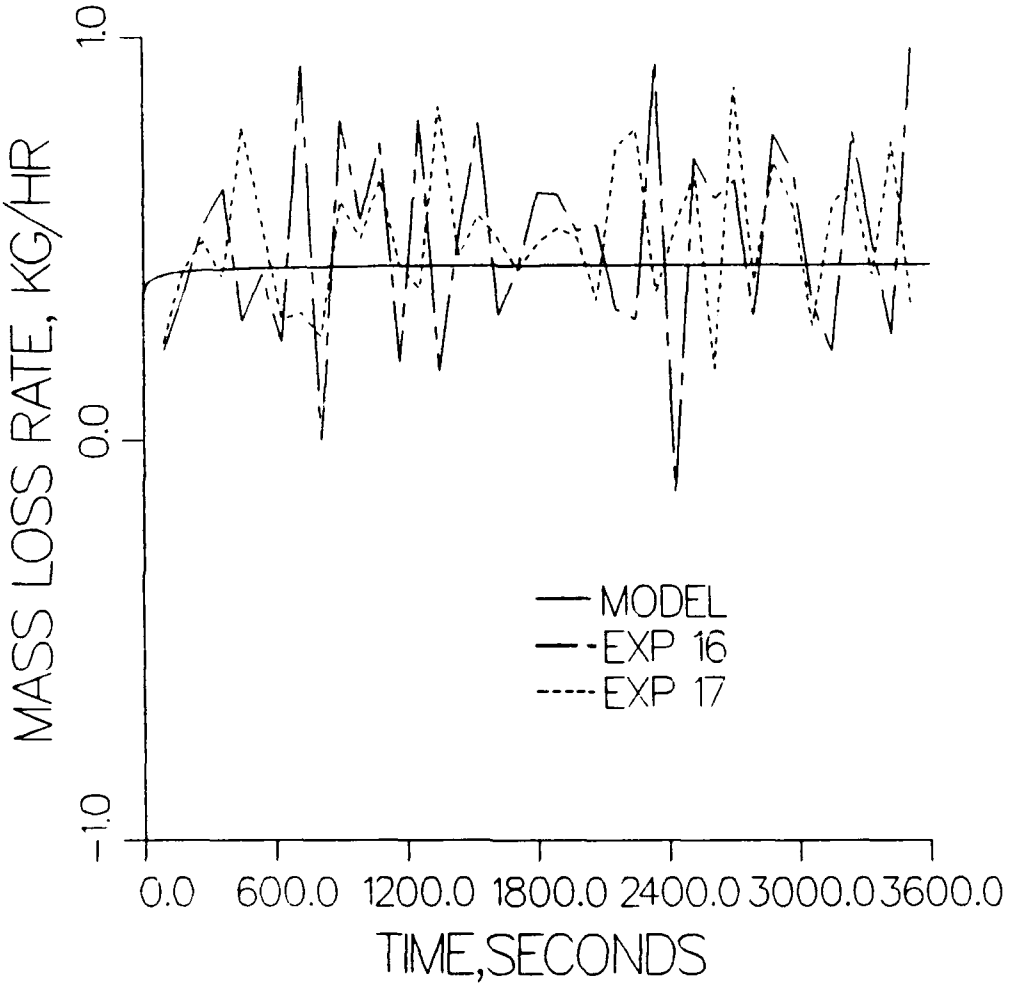

Figure 18. Model predictions versus results from open top experiments.

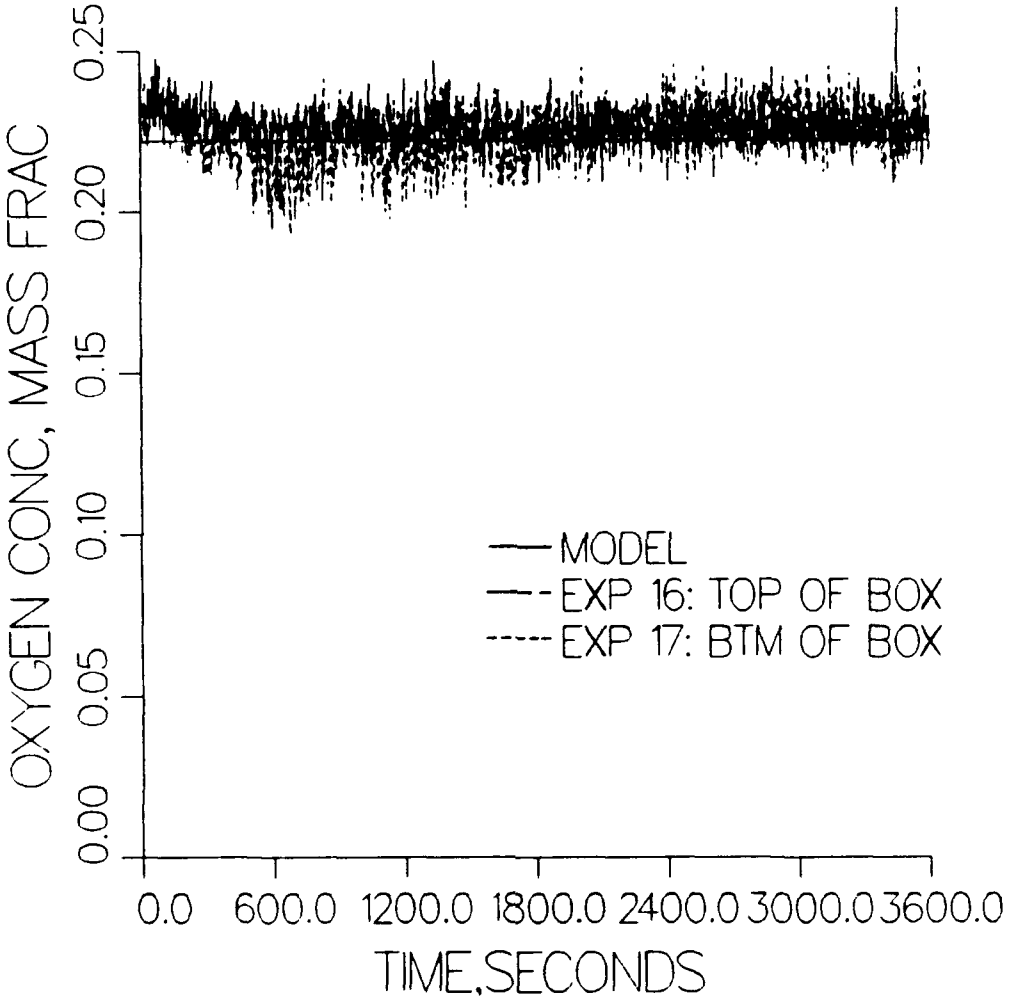

Figure 19. Model predictions versus results from open top experiments.

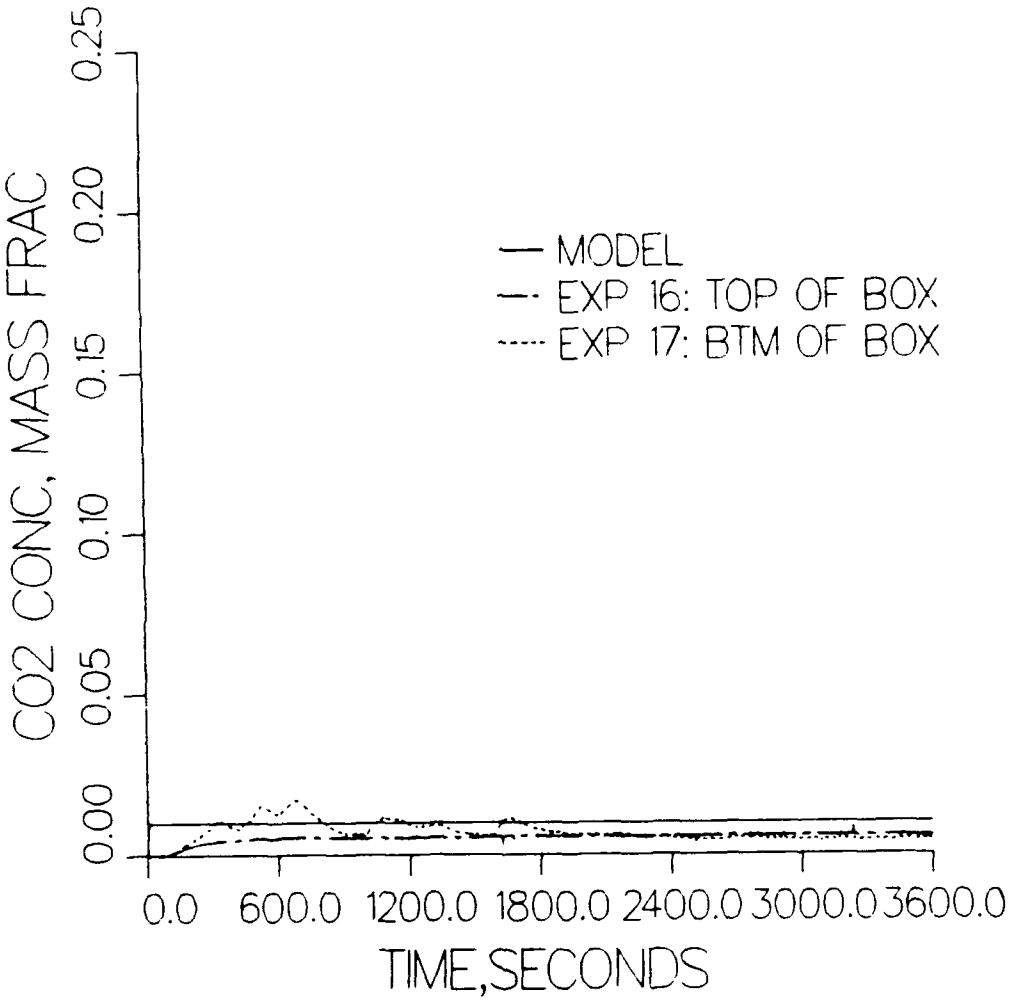

Figure 20. Model predictions versus results from open top experiments.

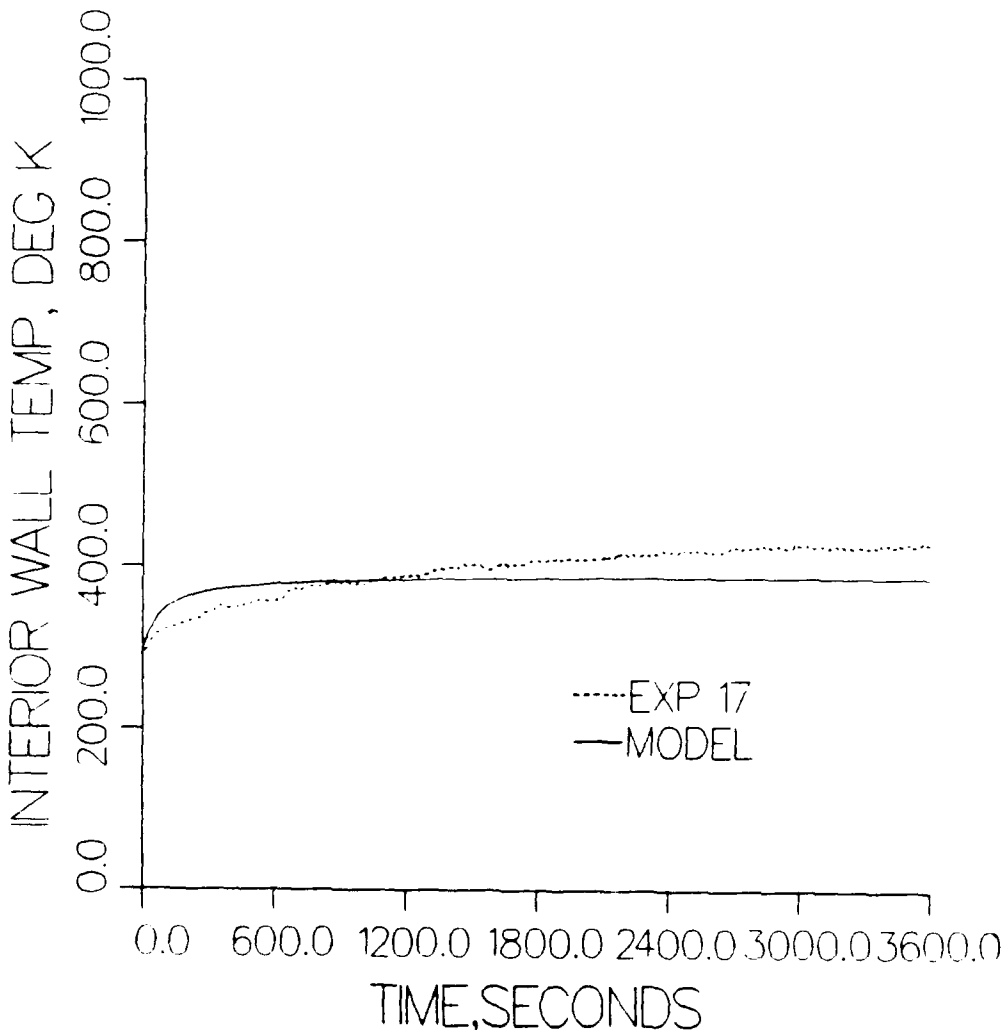

Figure 21. Model predictions versus results from open top experiments.

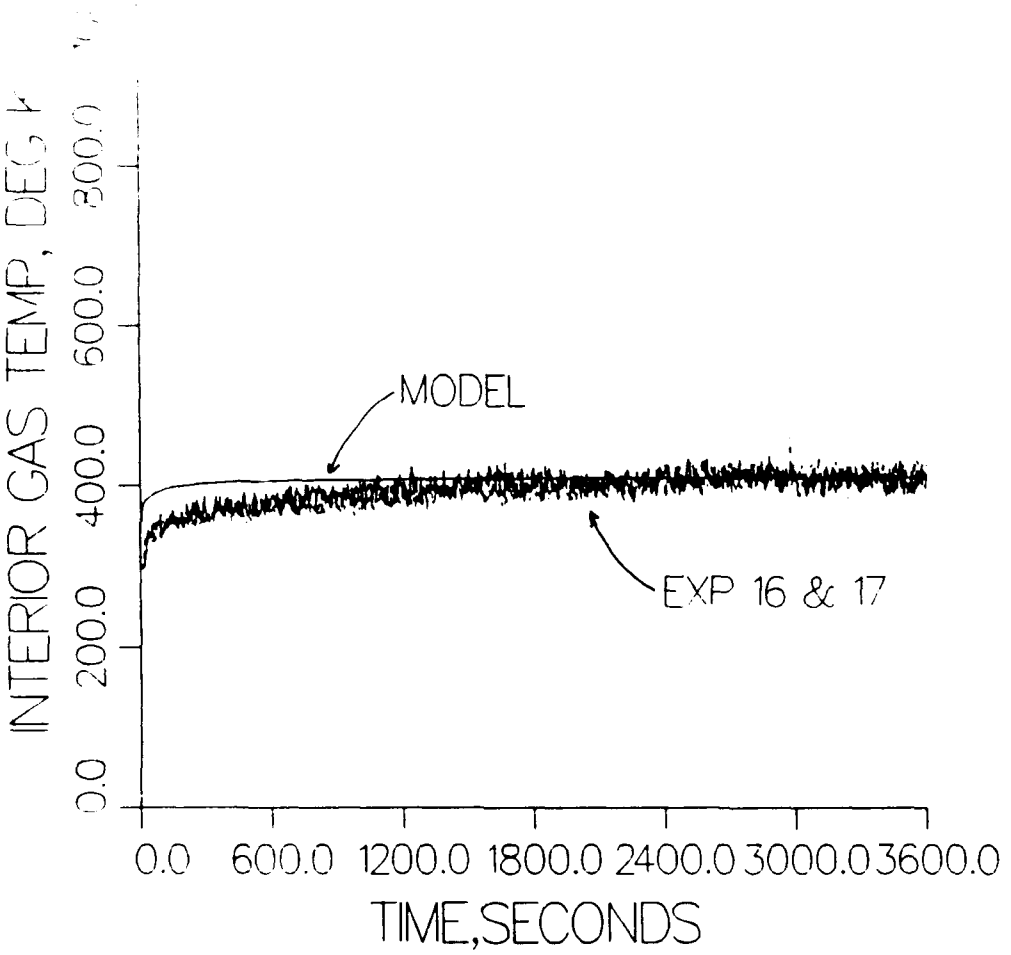

Figure 22. Model predictions versus results from open top experiments.

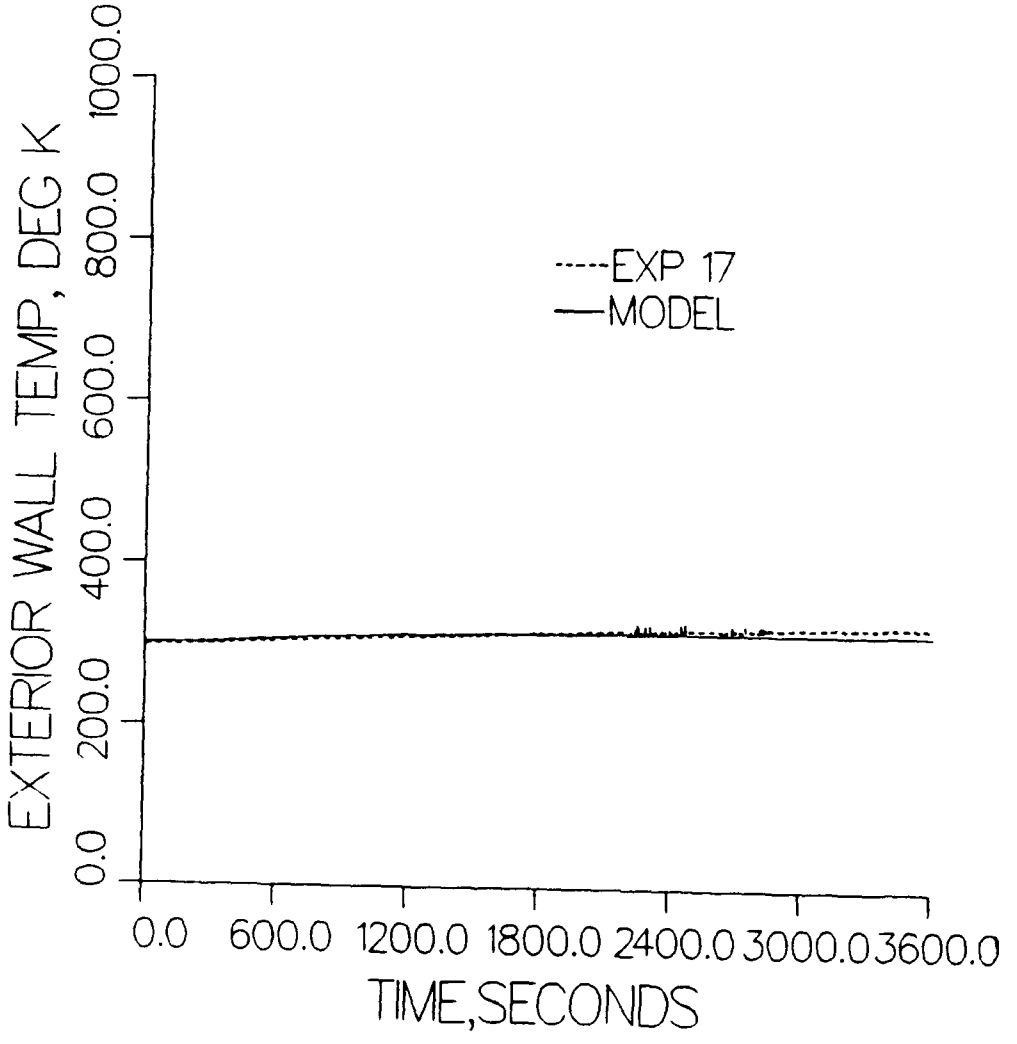

Figure 23. Model predictions versus results from open top experiments.